Chemical Engineering Journal 162 (2010) 1026–1034

Contents lists available at ScienceDirect

Chemical Engineering Journal

journal homepage: www.elsevier.com/locate/cej

Study of removal of azo dye by functionalized multi walled carbon nanotubes

Ashish Kumar Mishra, T. Arockiadoss, S. Ramaprabhu*

Alternative Energy and Nanotechnology Laboratory (AENL), Nano Functional Materials Technology Centre (NFMTC), Department of Physics, Indian Institute of Technology Madras, Chennai 600036, India

ARTICLE INFO

Article history:
Received 22 March 2010
Received in revised form 2 July 2010
Accepted 6 July 2010

Keywords:
Dye removal
Functionalized MWNTs
Adsorption isotherm
Kinetic study
pH variation

ABSTRACT

Textile industries are one of the main sources of water pollution. Wastewater containing dyes present a serious environmental problem because of its high toxicity and possible accumulation in the environment. Azo dyes are the main class of dyes among all dyes. In the present work, functionalized multi walled carbon nanotubes (*f*-MWNTs) have been used for the adsorption (decolorization) of three different azoic dyes. Multiwalled carbon nanotubes (MWNTs) were synthesized by chemical vapor deposition (CVD) technique and purified by air oxidation and acid treatment. These purified MWNTs were further functionalized by acid treatment. Different characterization techniques like Electron microscopy, Raman and FTIR spectroscopy have been used to study the adsorption of azoic dyes over *f*-MWNTs surface. UV–visible absorption spectroscopy was used to quantify the decolorization of dyes. Adsorption isotherm and kinetic behaviors of *f*-MWNTs for azoic dyes removal were studied and fitted to different existing models. Maximum adsorption capacity of 148, 152 and 141 mg/g was obtained for direct congo red, reactive green HE4BD and golden yellow MR dyes, respectively. In addition effect of initial pH of dye solution and initial concentration of dye solution on adsorption property of *f*-MWNTs were studied.

1. Introduction

The textile industry is characterized by its high water consumption and is one of the largest producers of industrial wastewater. The main pollution sources of textile wastewater are the dyeing and finishing processes. Wastewater containing dyes present a serious environmental problem because of its high toxicity and possible accumulation in the environment. Most of these dyes are synthetic in nature and are classified based on their chemical structures into 6 different classes as azo, anthraquinone, sulfur, indigoid, triphenylmethane and phthalocyanine derivatives. Most of these dyes contain aromatic rings, which make them carcinogenic and mutagenic [1,2]. Dyes containing –N=N– group, are known as azo dyes. Due to the extensive use of these dyes in industries, they become an integral part of industrial wastewater. Therefore, the removal of dyes from textile effluents is currently of great interest. Various physical and chemical methods of treatment of industrial wastewater have been suggested, these include adsorption methods, coagulation processes, photocatalytic degradation and the ozone and hypochlorite treatment of dye waste effluents [3–5]. Among the advanced chemical or physical treatments, adsorption is considered to be superior to other techniques. This is attributed to its easy availability, simplicity of design, ease of operation, biodegradability, insensitivity to toxic substances and ability to treat dyes in more concentrated forms. Physical adsorption has been proven to be the most efficient method for quickly lowering the concentration of dissolved dyes in an effluent. In this regard, activated carbon is the most widely used adsorbent for removal of dyes from the aqueous solution [6,7], but it presents some disadvantages. It is flammable and difficult to regenerate as it needs to be reclaimed. Also, carbon could show it to be weakly hydrophilic, resulting in the weak affinity for the adsorption of cationic or anionic dyes from the aqueous solution. Carbon nanotubes (CNTs) are highly popular due to their novel properties like high aspect ratio, high thermal, electrical and mechanical properties [8–11]. High aspect ratio of CNTs, makes them a possible candidate for water purification. Large surface area and high porosity provide enough adsorption sites for harmful cations, anions and other organic and inorganic impurities present in some natural sources of water.

The outer surface of individual CNTs provides evenly distributed hydrophobic sites for organic chemicals. Different literatures suggest that hydrophobic interactions cannot completely explain the interaction between organic chemicals and CNTs. Other mechanisms include π–π interactions between bulk π systems on CNT surfaces and organic molecules with C=C double bonds or benzene rings), hydrogen bonds (because of the functional groups on CNT surfaces), and electrostatic interactions (because of the charged CNT surface) [12,13]. Long and Yang [14] reported that MWNTs could be more efficient for the removal of dioxin than

* Corresponding author. Tel.: +91 44 22574862; fax: +91 44 22570509.
E-mail address: ramp@iitm.ac.in (S. Ramaprabhu).

1385-8947/$ – see front matter © 2010 Elsevier B.V. All rights reserved.
doi:10.1016/j.cej.2010.07.014

Table 1
Properties of all the three azoic dyes.

Dye adsorbed	Formula	Molecular weight (g/mol)	Maximum adsorption wavelength (nm)
Direct congo red	$C_{32}H_{22}N_6O_6S_2Na_2$	696.7	488
Reactive green HE4BD	$C_{40}H_{35}Cl_2N_{15}O_{19}S_6$	1292	608
Golden yellow MR	$C_{18}H_{15}N_6O_2Cl$	382.5	422

activated carbon. Cai et al. [15] prepared a CNT-packed cartridge for the solid-phase extraction of compounds such as bis phenol A and 4-*c*-nonylphenol in environmental water samples. Li et al. [16,17] found that after oxidation with nitric acid, CNTs showed exceptional adsorption capability and high adsorption efficiency for Cd^{2+}, Cu^{2+} and Pb^{2+} removal from water. The above-mentioned work suggests that CNTs may have great application potential as an effective absorbent for the removal of organic and inorganic contaminants in environmental protection. However, until now little study is done on adsorption of dyes to CNTs [18]. Functionalized CNTs are hydrophilic in nature resulting in the high affinity for the adsorption of cations and anions from the aqueous solution due to the presence of oxygen containing functional groups at the surface and hence it is advantageous over activated carbon. Fornasieroa et al. [19] reported that electrostatic interactions dominate over steric effects in governing ion rejection with functionalized CNTs. This suggests that the rejection mechanism can play important role for anionic dyes removal using functionalized CNTs. Taking advantage of the large surface area and the hydrophilic nature of *f*-MWNTs, in the present work, *f*-MWNTs have been used for the adsorption (decolorization) of three different azoic dyes (direct congo red, reactive green HE4BD and golden yellow MR) and the adsorption has been confirmed by different characterization techniques. The maximum adsorption capacity and the effect of initial pH of dye solution and initial concentration of dye solution on adsorption property of *f*-MWNTs were studied and discussed.

2. Experimental

2.1. Materials and methods

Different azoic dyes (direct congo red, reactive green HE4BD and golden yellow MR) were purchased from Sri Palaniandaver Dyes & Chemicals, Erode, India. Chemical structure of above mentioned dyes are given in Fig. 1 [20–22]. Formula, molecular weight and maximum adsorption wavelength of the dyes are mentioned in Table 1. Solutions of 20 mL for each dye in de-ionized water and 50 mg of *f*-MWNTs were used for isotherm and kinetic studies as well as for study of variation in initial pH of the dye solution. To study the isotherm, kinetic and pH behavior batch experiments were performed. In this method, *f*-MWNTs were deposited as layer above cotton in a glass column. Different glass columns were prepared with equal amount of *f*-MWNTs and equal amount of varying concentration of dye solutions was treated for adsorption studies. Adsorption isotherms studies were performed with initial concentrations of dyes varying from 50 to 400 mg/L. Kinetic studies were performed with 400 mg/L concentration of dye solution. To study the pH variations, experiments were performed with initial concentration of 250 mg/L for dye solutions.

2.2. Synthesis of functionalized MWNTs

MWNTs were synthesized by catalytic chemical vapor deposition method. In this method hydrogen decrepitated AB_3 alloy was taken as catalyst material. Pyrolysis of acetylene takes place at 700 °C under inert atmosphere, which results in the growth of MWNTs [23]. These MWNTs were further purified by air oxidation followed by acid treatment to remove amorphous carbon and catalytic impurities. Purified MWNTs were further functionalized to make them hydrophilic by stirring MWNTs in conc. HNO_3 acid (16 M) for 2 h [24].

2.3. Characterization

Morphology of *f*-MWNTs was characterized by FEI QUANTA 200 Scanning Electron Microscope and JEOL 3010 High Resolution Transmission Electron Microscope. To study the pore size distribution and homogeneity of MWNTs surface, BET measurements were performed by Micromeritics ASAP 2020 analyzer. To study the vibrational characteristics of *f*-MWNTs and dye adsorbed *f*-MWNTs, Raman and FTIR analysis were performed. Raman analysis was performed by using HORIBA JOBIN YVON HR800UV Confocal Raman Spectrometer, while FTIR study was performed by using PERKINELMER Spectrum One FT-IR spectrometer. Quantification of decolorization for dyes was studied by using absorption spectroscopy. JASCO, V-570 UV–visible spectrophotometer was used for the above purpose.

3. Results and discussion

3.1. Microscopy analysis

TEM and SEM images (Fig. 2a and b) show the morphological structure of MWNTs. Images clearly suggests the crystalline tubular structure of nanotubes. The inner diameter (ID) and the outer diameter (OD) of the MWNTs are in the ranges of 5–10 nm and 40–50 nm, respectively. Fig. 2c and d shows the TEM and SEM images of dye adsorbed *f*-MWNTs. Clusters of adsorbed dye (direct congo red) over *f*-MWNTs surface can be seen from the images.

3.2. BET analysis

BET surface area measurement of purified MWNTs is shown in Fig. 3. Fig. 3a shows the nearly uniform pore size with the pore volume of 0.22 cm^3/g and pore radius in the range 1.7–2.5 nm. Pore volume was calculated by using BJH method. Fig. 3b shows the large hysteresis area of N_2 adsorption–desorption isotherm, which suggests the wide distributions of pores. The specific surface area of purified MWNTs calculated by using BET equation is found to be 91.96 m^2/g. The large hysteresis area indicates the nearly uniform distribution of pores and large surface area of purified MWNTs, suggests the high quality of synthesized MWNTs.

3.3. Raman spectrogram analysis

Raman spectroscopic analysis of *f*-MWNTs, individual dyes and individual dyes adsorbed *f*-MWNTs has been shown in the Fig. 4. Fig. 4 shows the comparative intensity of D-band (1337 cm^{-1}) with G-band (1571 cm^{-1}) for *f*-MWNTs, which arises because of further acid treatment of purified MWNTs, which leads to the defects on the surface of MWNTs due to the attachment of functional groups. In addition, a 2D-band occurs at 2673 cm^{-1}, which is the second harmonic of D-band. This attachment of functional groups at the surface of MWNTs provides hydrophilic nature to MWNTs [25]. Raman spectra of individual dyes show broadening at high Raman shift values, which may be attributed to the fluorescence effect. Dye

(a) Direct congo red

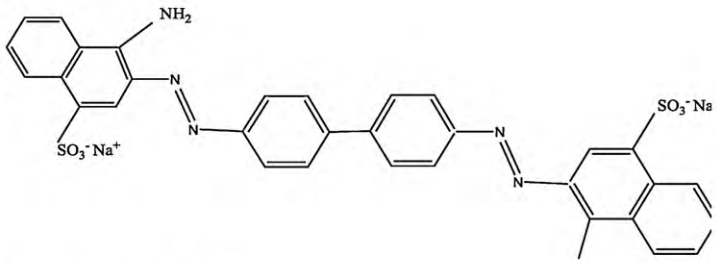

(b) Reactive green HE4BD

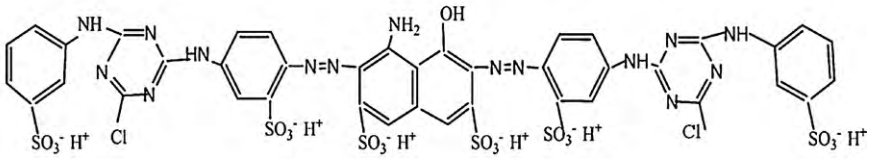

(c) Golden yellow MR

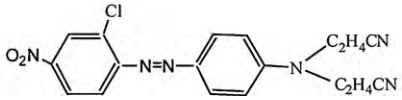

Fig. 1. Chemical structure of (a) direct congo red, (b) reactive green HE4BD and (c) golden yellow MR dyes.

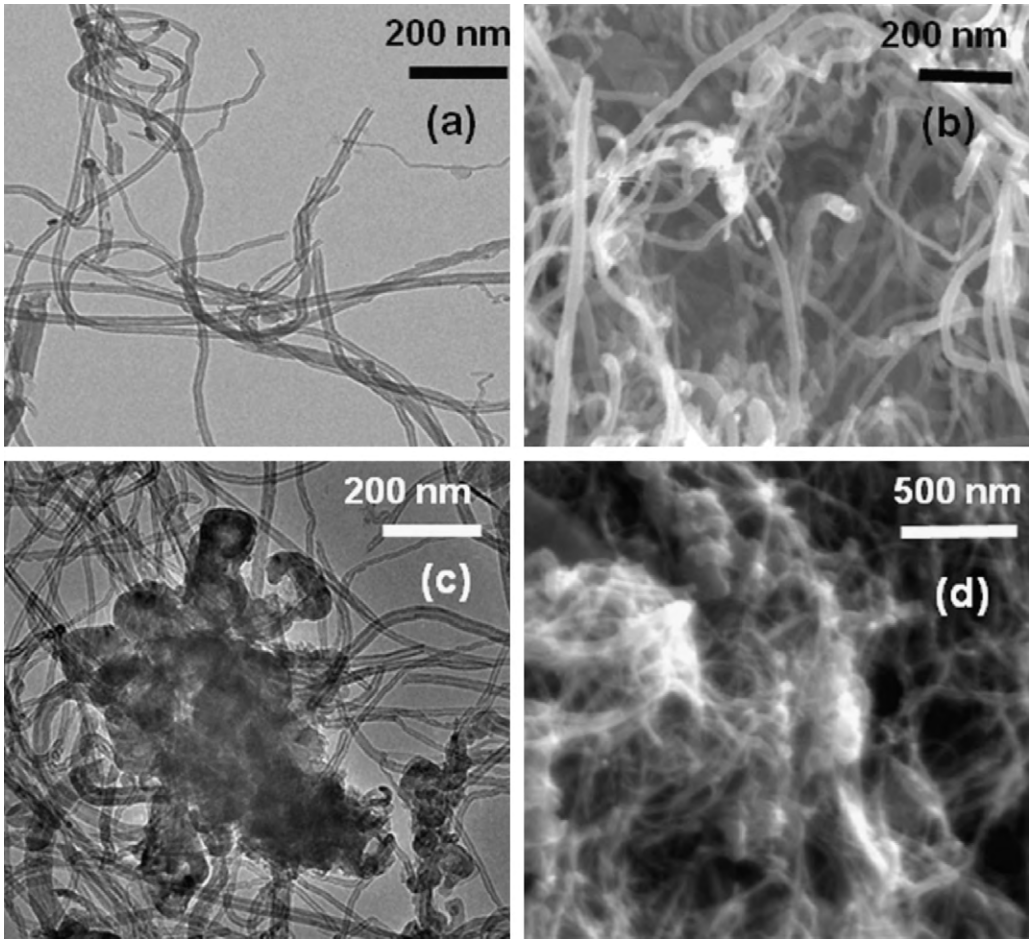

Fig. 2. TEM and SEM images of (a and b) *f*-MWNTs and (c and d) direct congo red adsorbed *f*-MWNTs.

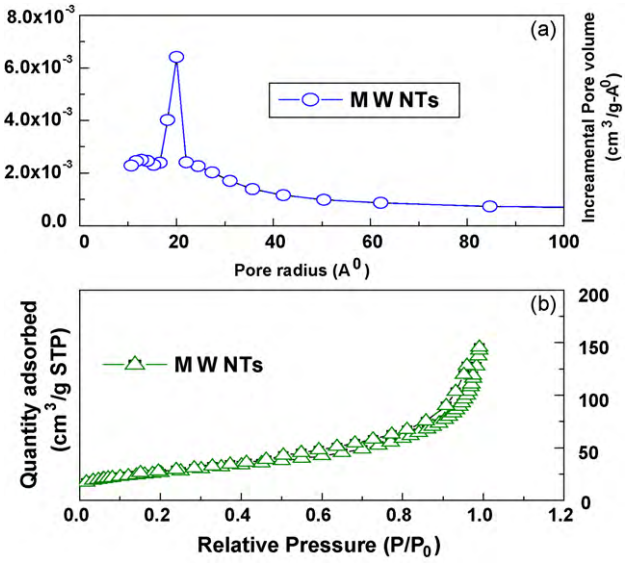

Fig. 3. BET measurements of MWNTs (a) pore size measurements and (b) N_2 adsorption–desorption isotherm based surface area measurement.

adsorbed *f*-MWNTs shows a shift in position of D-band, G-band and 2D-band to higher Raman shift values. The strong attachment of the dye to *f*-MWNTs may induce the observed up shift of the Raman characteristic peaks due to the increase in the elastic constant of the harmonic oscillator of the dye-adsorbed *f*-MWNTs. The van der Waals attraction between the dye and the graphite sheets of nanotubes may increase the energy necessary for vibrations to occur, which is reflected in the higher frequency of Raman peaks [26,27]. In case of direct red and reactive green adsorbed *f*-MWNTs (Fig. 4a and b) peak shift was found more compared to the golden yellow adsorbed *f*-MWNTs (Fig. 4c). This may attribute to the presence of ions in direct red and reactive green dyes, respectively, which includes the electrostatic interaction between dye and *f*-MWNTs along with van der Waals interaction.

3.4. Fourier transform infrared spectrogram analysis

Fourier transform infrared spectroscopic analysis of *f*-MWNTs, dyes and different dyes adsorbed MWNTs has been shown in Fig. 5. FTIR study of *f*-MWNTs confirms the defective sites at the surface of *f*-MWNTs and the presence of >C=C (1635 cm^{-1}), >C=O (1022 cm^{-1}), $=CH_2$ (2854, 2925 cm^{-1}) and –OH (3437 cm^{-1}) functional groups at the surface of MWNTs. This leads to the hydrophilic nature of MWNTs. These functional groups may also act as anchoring sites for dye molecules. In the case of direct red dye, peaks at 1065, 1180, 1226, 1364 and 1447 cm^{-1} correspond to sulfonate containing group of dye and C–H parallel bending of aromatic rings of direct red dye, while peak at 1611 cm^{-1} corresponds to –N=N– group. Peak at 3466 cm^{-1} corresponds to amine group attached to the aromatic ring. In case of direct red dye adsorbed *f*-MWNTs, additional peaks was found at 1459 cm^{-1} may correspond to the sulfonate group of dye adsorbed on *f*-MWNTs surface and shift in 1022 cm^{-1} peak (now at 1041 cm^{-1}) were observed which may correspond to the attachment of direct red dye at *f*-MWNTs surface (Fig. 5a). In case of reactive green dye, peaks at 1045, 1132, 1286 and 1489 cm^{-1} correspond to the sulfonate containing group of dye and C–H parallel bending of aromatic rings of reactive green dye, while peak at 1578 cm^{-1} corresponds to –N=N– group and peak at 3434 cm^{-1} corresponds to alcoholic and amine group attached to the aromatic rings of the dye molecule. FTIR spectra of reactive green adsorbed *f*-MWNTs show additional peaks at 1120 and 1458 cm^{-1}, which may correspond to the sulfonate group of reactive green dye adsorbed on *f*-MWNTs surface. A shift in 1022 cm^{-1} peak (now at 1041 cm^{-1}) was observed, which may correspond to the attachment of dye at *f*-MWNTs surface (Fig. 5b). In case of golden yellow dye, peaks at 1630 cm^{-1} arises due to –N=N– group, 1523 cm^{-1} due to $–NO_2$ group attached to the aromatic ring of golden yellow dye and 1375 cm^{-1} due to $–NR_2$ attached to the

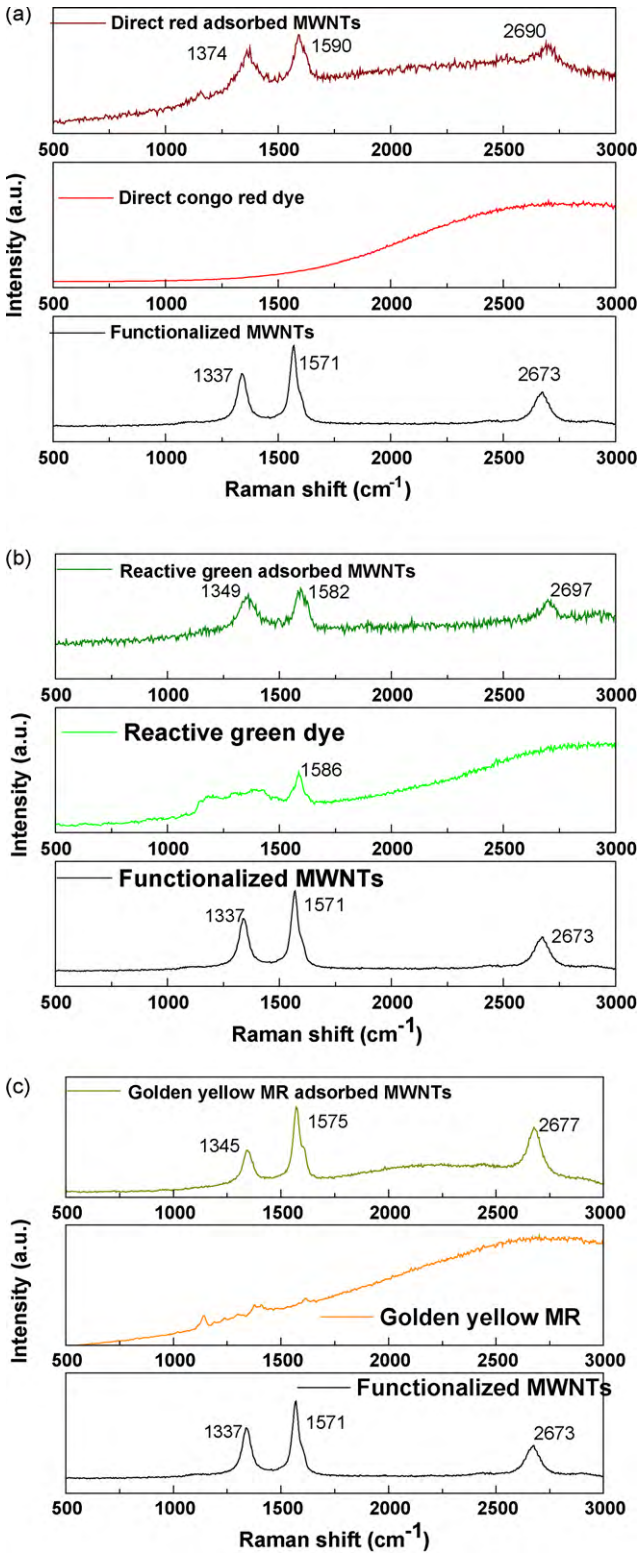

Fig. 4. Raman spectra of *f*-MWNTs and (a) direct congo red, (b) reactive green HE4BD and (c) golden yellow MR dyes adsorbed *f*-MWNTs.

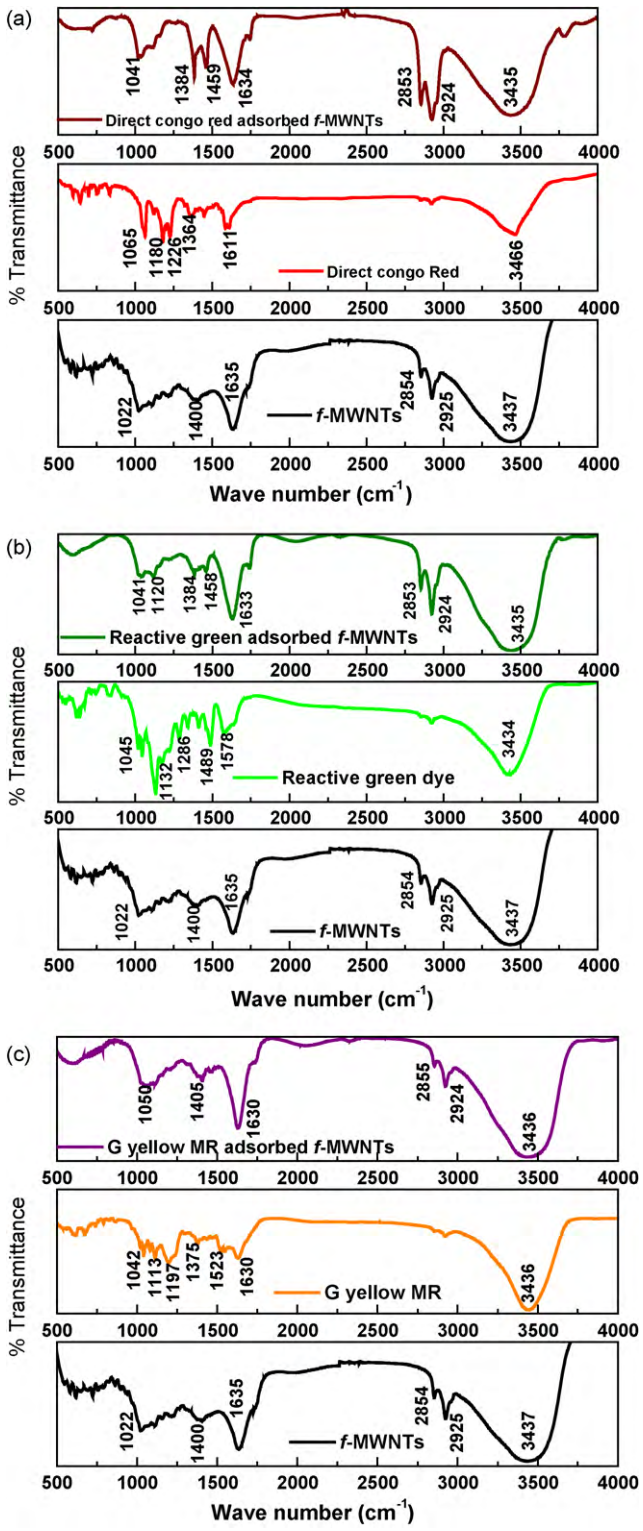

Fig. 5. FTIR spectra of *f*-MWNTs and (a) direct congo red, (b) reactive green HE4BD and (c) golden yellow MR dyes adsorbed *f*-MWNTs.

aromatic ring of the corresponding dye. Peaks at 1042, 1113 and 1197 cm^{-1} may arise due to the halogen (chlorine) attached to the aromatic ring and C–H parallel bending of aromatic rings of golden yellow dye. FTIR spectra of golden yellow dye adsorbed *f*-MWNTs show a broad peak around 1050 cm^{-1} and small shift in 1400 cm^{-1} (now at 1405 cm^{-1}) compared to *f*-MWNTs, which may arise due to the attachment of golden yellow dye at *f*-MWNTs surface (Fig. 5c)

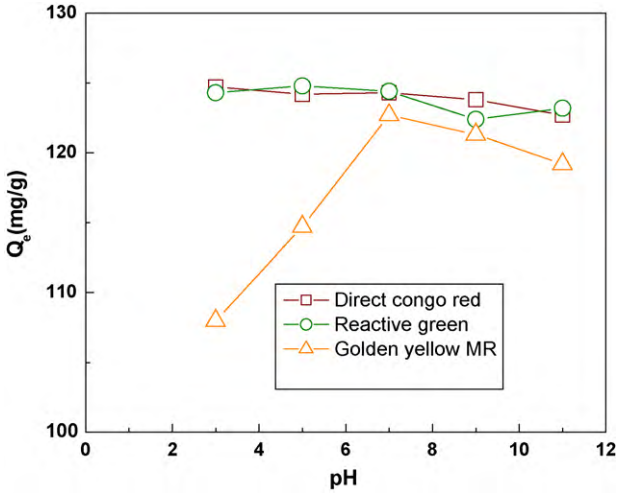

Fig. 6. Effect of initial pH on azoic dyes adsorption with 250 mg/L initial concentration of dye solutions.

[25,28,29]. Thus the presence of extra peaks and shift in peaks of dye adsorbed *f*-MWNTs compared to *f*-MWNTs shows the adsorption of dyes over *f*-MWNTs surface. This suggests the strong interaction between dye molecules and *f*-MWNTs surface and hence suggesting *f*-MWNTs as an appropriate adsorbent for dyes.

3.5. Study of initial pH

The influence of pH on the removal of azoic dyes by *f*-MWNTs was studied to gain further insight into the adsorption process. Fig. 6 shows the effect of initial pH on the removal of all the three azoic dye solutions by *f*-MWNTs. The effect of pH was observed over the pH range 3–11 with 250 mg/L initial concentration of dye. It was observed that removal of direct congo red and reactive green is less sensitive with initial pH variation of the dye solution compared to the removal of golden yellow MR. In case of direct red maximum dye removal was found at pH 3 and reported optimum range for direct red is pH 2–4. In case of reactive green maximum dye removal was at pH 5, while for golden yellow MR it was at pH 7. More adsorption was observed for direct red and reactive green compared to golden yellow dye. This may attribute to the electrostatic interaction between anionic dyes (direct red and reactive green) and partially negative charged *f*-MWNTs surface due to the presence of oxygen containing functional groups. Fornasieroa et al. [19] reported that electrostatic interactions dominate in governing ion rejection with functionalized CNTs from aqueous solution. Maximum adsorption capacities of 124.7 (at pH 3), 124.8 (at pH 5) and 122.7 mg/g (at pH 7) were observed for direct red, reactive green and golden yellow dyes, respectively.

3.6. Adsorption isotherm studies

The quantity of the dye that could be adsorbed over *f*-MWNTs surface is a function of concentration, which could be explained by adsorption isotherms. In the present study, Langmuir [30], Freundlich [31] and Temkin [32] isotherms were tested for different dyes adsorption. Langmuir isotherm assumes that the single adsorbate binds to a single site on the adsorbent and that all surface sites on the adsorbents have the same affinity for the adsorbate. Langmuir isotherm is represented by the following equation

$$Q_e = \frac{abC_e}{1 + bC_e} \quad (1)$$

Table 2
Isotherm constants for azoic dyes.

Dye adsorbed	Langmuir constants	Freundlich constant	Temkin constant
Direct congo red	a = 148.0859 mg/g b = 0.5599 L/g R^2 = 0.97116	k = 57.39552 (mg/g)(L/mg)$^{1/n}$ n = 3.01569 R^2 = 0.98482	B = 25.05076 K_T = 12.8069 (L/mg) R^2 = 0.97461
Reactive green HE4BD	a = 151.8865 mg/g b = 0.44675 L/g R^2 = 0.98955	k = 51.83082 (mg/g)(L/mg)$^{1/n}$ n = 2.80126 R^2 = 0.93006	B = 32.20612 K_T = 4.43176 (L/mg) R^2 = 0.98704
Golden yellow MR	a = 141.618 mg/g b = 0.52456 L/g R^2 = 0.99484	k = 54.63815 (mg/g)(L/mg)$^{1/n}$ n = 3.4484 R^2 = 0.89839	B = 27.1227 K_T = 6.47472 (L/mg) R^2 = 0.97405

Table 3
Comparative study of maximum adsorption capacity of different adsorbents.

Adsorbent	Adsorbate	Maximum adsorption capacity (mg/g)	References
Waste Fe(III)/Cr(III) hydroxide	Congo Red	~44	[31]
Bagasse fly ash	Congo Red	~12	[32]
Activated red mud	Congo Red	~7	[33]
Activated cotton seed shells	Acid Red 114	~153	[8]
MWNTs	Congo Red	148	Present work
Activated carbon	Reactive Yellow 15	~116	[34]
Activated rice husk carbon	Acid Yellow 36	86.9	[35]
Commercial activated carbon	Acid Yellow 23	56.5	[36]
Calcined alunite	Acid yellow 17	151.5	[5]
MWNTs	Golden yellow MR	141	Present work
Carbonaceous material	Basic green 4	~75.1	[5]
Sugarcane dust	Basic green 4	~4	[5]
Oil palm trunk fiber	Basic green 4	~149.4	[5]
MWNTs	Reactive green HE4BD	152	Present work

The Freundlich isotherm can be derived from the Langmuir isotherm by assuming that there exists a distribution of sites on the adsorbents for different adsorbates with each site behaving accordingly to the Langmuir isotherm. Freundlich isotherm is represented by the following equation

$$Q_e = k(C_e)^{\frac{1}{n}} \quad (2)$$

Temkin isotherm is represented by the following equation

$$Q_e = B \ln K_T + B \ln C_e \quad (3)$$

where 'Q_e' is the amount of dye adsorbed per unit weight of adsorbent (mg/g), 'C_e' is the equilibrium concentration of dye solution (mg/L), 'b' is the constant related to the free energy of adsorption (L/mg) and 'a' is maximum adsorption capacity. 'k' is the Freundlich constant indicative of the relative adsorption capacity of the adsorbent (mg/g) and ($1/n$) is the adsorption intensity. 'K_T' is the equilibrium binding constant (mg^{-1}) and 'B' is the heat of adsorption. 'Q_e' is calculated by the following formula

$$Q_e = \frac{(C_0 - C_e)V}{m} \quad (4)$$

where 'C_0' is the initial concentration of dye solution, 'V' is the volume of dye solution and 'm' is the mass of adsorbent. All the above-mentioned isotherms were studied for three different dyes and isotherm constants were calculated by using the corresponding equations. Fig. 7 shows the comparative plot mentioned isotherms for all the three dyes. Isotherm constants and the correlation factors are given in Table 2. For the experimental results, it is clear that the adsorption follows Langmuir, Freundlich and Temkin models for all the three azo dyes. The maximum adsorption capacities (Langmuir constant a) of MWNTs were found to be 148, 152 and 141 mg/g for direct red, reactive green and golden yellow dye, respectively, which are higher than some of the earlier reported values for different dyes in review article by Gupta and Suhas [4]. Comparative values of maximum adsorption capacity for some of the adsorbents for different dyes removal are given in Table 3 [5–7,33–38]. The presence of oxygen containing functional groups also imparts a partial negative charge to the *f*-MWNTs surface, which can increase the preferential adsorption of anionic dye molecules by the rejection mechanism explained by Fornasieroa et al. [19]. Adsorption mech-

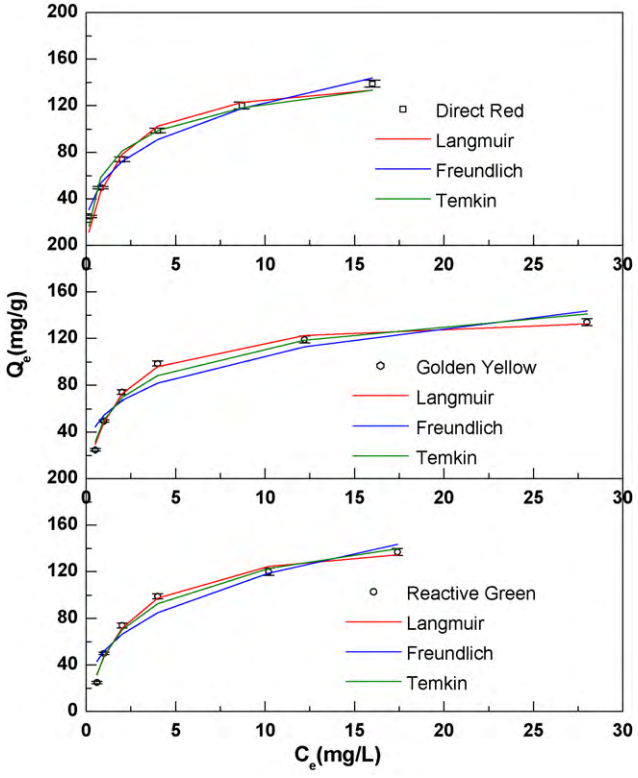

Fig. 7. Isotherm study of azoic dye adsorption with varying initial concentration from 50 to 400 mg/L of dye solution.

Table 4
Kinetic constants for azoic dyes.

Dye adsorbed	Pseudo first order constants	Pseudo second order constants
Direct congo red	Q_e = 177.777 (mg/g) K_1 = 0.03153 (min^{-1}) R^2 = 0.99406	Q_e = 277.4223 (mg/g) h = 2.4792 $K_2 = 0.032 \times 10^{-3}$ g/(mg min) R^2 = 0.96527
Reactive green HE4BD	Q_e = 163.9656 (mg/g) K_1 = .03324 (min^{-1}) R^2 = 0.99829	Q_e = 249.27815 (mg/g) h = 2.47397 $K_2 = 0.039 \times 10^{-3}$ g/(mg min) R^2 = 0.98757
Golden yellow MR	Q_e = 160.6082 (mg/g) K_1 = 0.02976 (min^{-1}) R^2 = 0.99892	Q_e = 250.2466 (mg/g) h = 2.12629 $K_2 = 0.034 \times 10^{-3}$ g/(mg min) R^2 = 0.97874

anisms include π–π interactions between bulk π systems on CNT surfaces and organic molecules with C=C double bonds or benzene rings), hydrogen bonds (because of the functional groups on CNT surfaces), and electrostatic interactions (because of the charged CNT surface) [12,13]. The values of $(1/n)$ for Freundlich model were found to be between 0 and 1, indicating the favorable adsorption of all the three azo dyes over *f*-MWNTs.

3.7. Kinetic studies

The transient behavior of the dye adsorption process was analyzed by using different kinetic models. Adsorption kinetic models are generally classified as adsorption reaction models and adsorption diffusion models. Pseudo first order and pseudo second order kinetic models are adsorption reaction models. Adsorption reaction model originates from chemical reaction kinetics. These above mentioned models were studied separately for all the three azo dyes adsorption. To study the adsorption kinetics of different dyes for *f*-MWNTs, 400 mg/L initial concentration of corresponding dye solutions were used.

The linear form of pseudo first order rate equation is

$$\ln(Q_e - Q_t) = \ln Q_e - \frac{K_1}{2.303}t \tag{5}$$

This equation can be modified in the following form

$$Q_t = Q_e\left[1 - \exp\left(\frac{-K_1 t}{2.303}\right)\right] \tag{6}$$

The linear form of pseudo second order model is given by

$$\frac{t}{Q_t} = \frac{1}{h} + \frac{1}{Q_e}t \tag{7}$$

where h is given by

$$h = K_2 Q_e^2 \tag{8}$$

where 'Q_e' and 'Q_t' are the amount of dye adsorbed on adsorbent at equilibrium and at various time t (mg/g), K_1 and K_2 are the rate constant for pseudo first and pseudo second order kinetic models respectively. Second order constant 'h' exhibits the initial adsorption rate (mg/g min) [39].

The comparative fits of both kinetic models for different adsorbates are shown in Fig. 8a and b. In the present study, it was observed that pseudo first order kinetics fit better for all the three azoic dyes compared to pseudo second order model. Fig. 8a clearly shows the reasonable fast kinetics of *f*-MWNTs for azoic dyes adsorption. The rate constants, predicted equilibrium uptakes and the corresponding correlations coefficient for all the three azoic dyes (adsorbates) are summarized in Table 4.

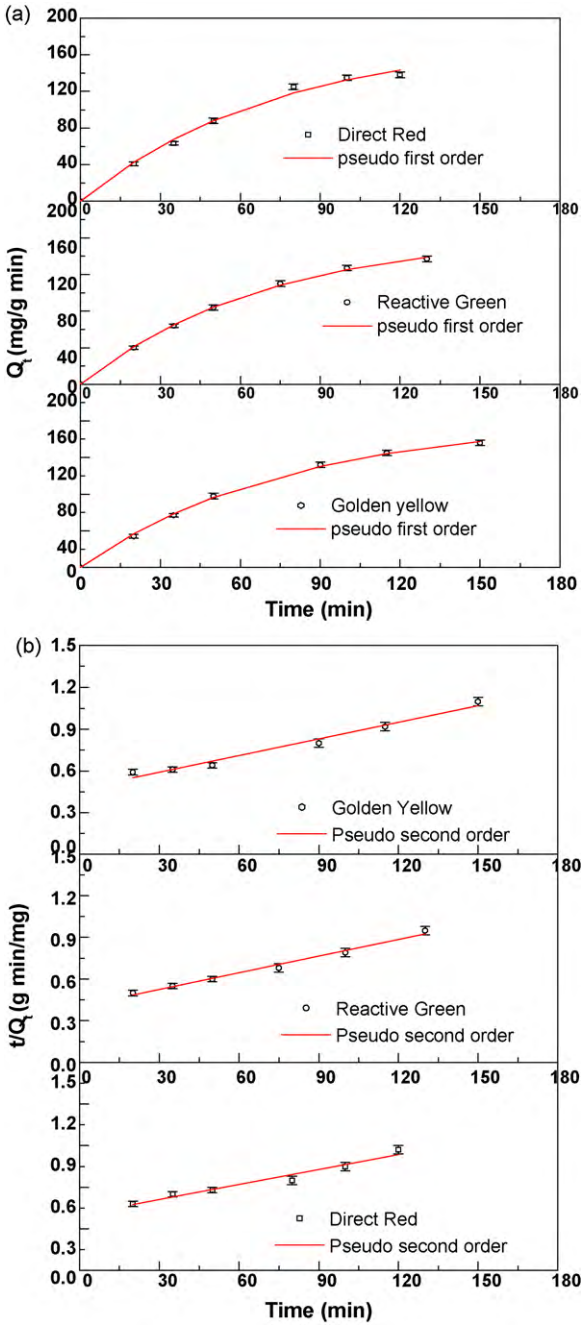

Fig. 8. (a) Pseudo first order and (b) pseudo second order kinetic studies of azoic dyes adsorption with 400 mg/L intial concentration of dye solution.

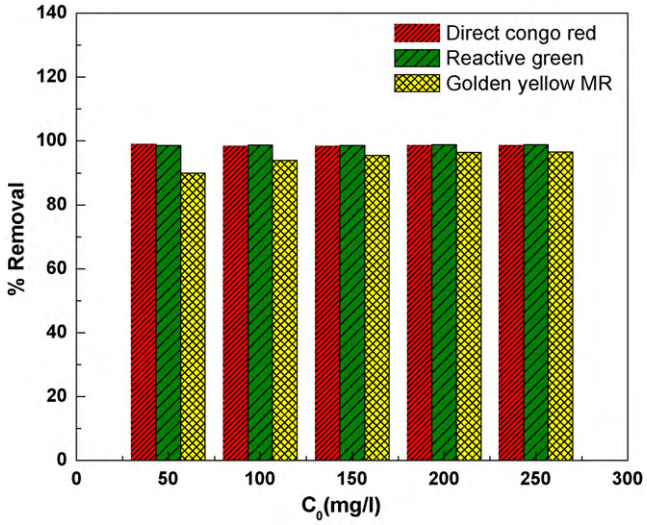

Fig. 9. Effect of initial adsorbate concentration on removal efficiency of *f*-MWNTs for azoic dyes.

3.8. Study of initial adsorbate concentration

Effect of initial concentration of dye solution on dye removal efficiency was studied. Removal efficiency in percentage was calculated using the following formula

$$\%\text{Removal efficiency} = \frac{(C_0 - C_f)100}{C_0} \quad (9)$$

where C_0 is the initial concentration of dye in solution and C_f is the final concentration of dye in solution after treatment. Effect of initial concentration of dye solution was studied in the range 50 to 250 mg/L. Maximum % removal of 98.6, 98.8 and 96.6 was observed for direct red, reactive green and golden yellow dyes respectively at the initial concentration of 250 mg/L for adsorbate (Fig. 9). In case of direct red and reactive green dyes removal efficiency was almost same for all studied initial concentrations, while removal efficiency for golden yellow MR increases with increase in initial concentration of dye in the range studied. This clearly suggests that *f*-MWNTs have more affinity for direct red and reactive green dye adsorption compared to golden yellow. This difference may be due to the possible electrostatic interaction (rejection between negatively charged *f*-MWNTs surface and anionic dyes) involved in earlier two dyes, which is absent in the golden yellow dye.

4. Conclusion

In the present study we have demonstrated *f*-MWNTs as novel adsorbent material for azoic dyes. More removal of anionic azo dye was observed with *f*-MWNTs which may be attributed to the involvement of electrostatic interaction between *f*-MWNTs surface and anionic azo dyes along with van der Waals interaction. Adsorption isotherms for all the three azoic dyes follow Langmuir, Freundlich and Temkin isotherms. Maximum adsorption capacities of *f*-MWNTs for all the three dyes were found more than most of the earlier reported values. Fast kinetics of *f*-MWNTs for azoic dyes adsorption were observed and kinetics behavior mainly follows pseudo first order model compared to pseudo second order model. Azoic dyes adsorption was found to be less sensitive with the variation in initial pH of the solution, suggesting its possible use in industrial wastewater treatment.

Acknowledgements

The authors acknowledge the supports of Alumni association, IITM and DST, India. One of the authors (Ashish) is thankful to DST India for providing the financial support. Authors are also thankful to Department of Chemistry and SAIF, IIT Madras for helping in BET and FTIR analysis.

References

[1] T. Robinson, G. McMullan, R. Marchant, P. Nigam, Remediation of dyes in textile effluent: a critical review on current treatment technologies with a proposed alternative, Bioresour. Technol. 77 (2001) 247–255.
[2] A. Mittal, J. Mittal, L. Kurup, Adsorption isotherms, kinetics and column operations for the removal of hazardous dye, tartrazine from aqueous solutions using waste materials-bottom ash and de-oiled soya, as adsorbents, J. Hazard. Mater. 136 (2006) 567–578.
[3] M.A. Behnajady, N. Modirshhla, N. Daneshvar, M. Rabbani, Photocatalytic degradation of an azo dye in a tubular continuous-flow photoreactor with immobilized TiO2 on glass plates, Chem. Eng. J. 127 (2007) 167–176.
[4] V.K. Gupta, Suhas, Application of low-cost adsorbents for dye removal—a review, J. Environ. Manage. 90 (2009) 2313–2342.
[5] M.A. Rauf, S.B. Bukallah, A. Hamadi, A. Sulaiman, F. Hammadi, The effect of operational parameters on the photoinduced decoloration of dyes using a hybrid catalyst V_2O_5/TiO_2, Chem. Eng. J 129 (2007) 167–172.
[6] A. Demirbas, Agricultural based activated carbons for the removal of dyes from aqueous solutions: a review, J. Hazard. Mater. 167 (2009) 1–9.
[7] X. Luo, L. Zhang, High effective adsorption of organic dyes on magnetic cellulose beads entrapping activated carbon, J. Hazard. Mater. 171 (2009) 340–347.
[8] S. Iijima, Helical microtubules of graphitic carbon, Nature 354 (1991) 56–58.
[9] R.B. Rakhi, K. Sethupathi, S. Ramaprabhu, Field emission from carbon nanotubes on a graphitized carbon fabric, Carbon 46 (2008) 1656–1663.
[10] A.L.M. Reddy, S. Ramaprabhu, Nanocrystalline Metal Oxides dispersed multiwalled carbon nanotubes as supercapacitor electrode, J. Phys. Chem. C 111 (2007) 7727–7734.
[11] N. Jha, S. Ramaprabhu, Thermal conductivity studies of metal dispersed multiwalled carbon nanotubes in water and ethylene glycol based nanofluids, J. Appl. Phys. 106 (2009) 084317–84326.
[12] D.H. Lin, B.S. Xing, Adsorption of phenolic compounds by carbon nanotubes: role of aromaticity and substitution of hydroxyl groups, Environ. Sci. Technol. 42 (2008) 7254–7259.
[13] B. Pan, B. Xing, Adsorption mechanisms of organic chemicals on carbon nanotubes, Environ. Sci. Technol. 42 (2008) 9005–9013.
[14] R.Q. Long, R. Yang, Carbon nanotubes as superior sorbent for dioxin removal, J. Am. Chem. Soc. 123 (2001) 2058–2059.
[15] Y. Cai, G. Jiang, J. Liu, Q. Zhou, Multiwalled carbon nanotubes as a solid-phase extraction adsorbent for the determination of bisphenol A, 4-*n*-nonylphenol, and 4-*tert*-octylphenol, Anal. Chem. 75 (2003) 2517–2521.
[16] Y.H. Li, S. Wang, Z. Luan, J. Ding, C. Xu, D. Wu, Adsorption of cadium (II) from aqueous solution by surface oxidized carbon nanotubes, Carbon 41 (2003) 1057–1062.
[17] Y.H. Li, J. Ding, Z. Luan, Z. Di, Y. Zhu, C. Xu, D. Wu, B. Wei, Competitive adsorption of Pb2+, Cu2+ and Cd2+ ions from aqueous solutions by multiwalled carbon nanotubes, Carbon 41 (2003) 2787–2792.
[18] C.H. Wu, Adsorption of reactive dye onto carbon nanotubes: equilibrium, kinetics and thermodynamics, J. Hazard. Mater. 144 (2007) 93–100.
[19] F. Fornasieroa, H.G. Parkb, J.K. Holta, M. Stadermanna, C.P. Grigoropoulosc, A. Noy, O. Bakajin, Ion exclusion by sub-2-nm carbon nanotube pores, PNAS 105 (2008) 17250–17255.
[20] R. Jain, S. Sikarwar, Removal of hazardous dye congo red from waste material, J. Hazard. Mater. 152 (2008) 942–948.
[21] M. Yılmaz, G. Bayramoglu, M.Y. Arıca, Separation and purification of lysozyme by reactive green 19 immobilised membrane affinity chromatography, Food Chem. 89 (2005) 11–18.
[22] J.F. Malone, S.J. Andrews, J.F. Bullock, R. Docherty, The solid state structure of CI disperse orange 44, Dyes Pigments 30 (1996) 183–200.
[23] M.M. Shaijumon, S. Ramaprabhu, Synthesis of carbon nanotubes by pyrolysis of acetylene using alloy hydride materials as catalysts and their hydrogen adsorption studies, Chem. Phys. Lett. 374 (2003) 513–520.
[24] X. Fiang, F. Gu, X. Bai, L. Lin, Y. Zhang, The influence of acid treatment on multiwalled carbon nanotubes, Pigment Resin Technol. 38 (2009) 165–173.
[25] U.J. Kim, C.A. Furtado, X. Liu, G. Chen, P.C. Eklund, Raman and IR spectroscopy of chemically processed single walled carbon nanotubes, J. Am. Chem. Soc. 268 (2005) 241–247.
[26] V.A. Sinani, M.K. Gheith, A.A. Yaroslavov, A.A. Rakhnyanskaya, K. Sun, A.A. Mamedov, J.P. Wicksted, N.A. Kotov, Aqueous dispersions of single-wall and multiwall carbon nanotubes with designed amphiphilic polycations, J. Am. Chem. Soc. 127 (2005) 3463–3472.
[27] C. Hu, H. Liao, F. Li, J. Xiang, W. Li, S. Duo, M. Li, Noncovalent functionalization of multi-walled carbon nanotubes with siloxane polyether copolymer, Mater. Lett. 62 (2008) 2585–2588.
[28] N.B. Colthup, Spectra-structure correlations in the infra-red region, J. Opt. Soc. Am. 40 (1950) 397–400.

[29] C.E. Meloan, Elementary Infrared Spectroscopy, first ed., Macmillan, New York, 1963.
[30] I. Langmuir, The adsorption of gases on plane surfaces of glass, mica and platinum, J. Am. Chem. Soc. 40 (1918) 1361–1403.
[31] H.M.F. Freundlich, Over the adsorption in solution, J. Phys. Chem. 57 (1906) 385–471.
[32] M.J. Temkin, V. Pyzhev, Kinetics of ammonia synthesis on promoted iron catalysts, Acta Physicochim. URSS 12 (1940) 217–222.
[33] C. Namasivayam, R. Jeyakumar, R.T. Yamuna, Dye removal from wastewater by adsorption on waste Fe(III)/Cr(III) hydroxide, Waste Manage. 14 (1994) 643–648.
[34] I.D. Mall, V.C. Srivastava, N.K. Agarwal, I.M. Mishra, Removal of congo red from aqueous solution by bagasse fly ash and activated carbon: kinetic study and equilibrium isotherm analyses, Chemosphere 61 (2005) 492–501.
[35] A. Tor, Y. Cengeloglu, Removal of congo red from aqueous solution by adsorption onto acid activated red mud, J. Hazard. Mater. 138 (2) (2006) 409–415.
[36] J.S. Macedo, N.B.C. Junior, L.E. Almeida, E.F.S. Vieira, A.R. Cestari, I.F. Gimenez, N.L.V. Carreno, L.S. Barreto, Kinetic and calorimetric study of the adsorption of dyes on mesoporous activated carbon prepared from coconut coir dust, J. Colloid Interface Sci. 298 (2) (2006) 515–522.
[37] P.K. Malik, Use of activated carbons prepared from sawdust and rice-husk for adsorption of acid dyes: a case study of acid yellow 36, Dyes Pigments 56 (239) (2003) e49.
[38] A.A. Attia, W.E. Rashwan, S.A. Khedr, Capacity of activated carbon in the removal of acid dyes subsequent to its thermal treatment, Dyes Pigments 69 (2006) 128–136.
[39] H. Qiu, B.C. Pan, Q.J. Zhang, W.M. Zhang, Q.X. Zhang, Critical review in adsorption kinetic models, J. Zhejiang Univ. Sci. A 10 (2009) 716–724.